iScience

CellPress
OPEN ACCESS

Article

Transition-State Expansion: A Quantitative Model for Counterion Effects in Ionic Reactions

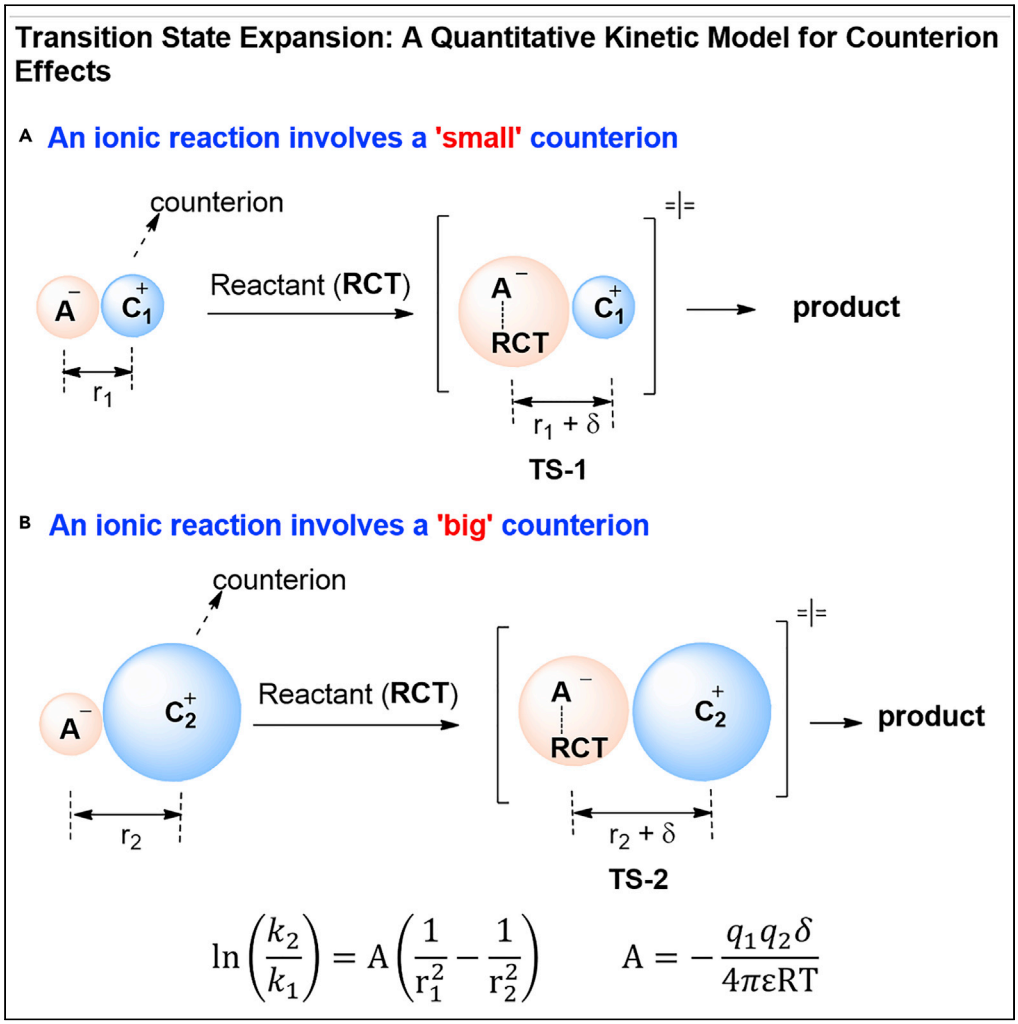

Junbin Han, Zhichao Lu, Gerald B. Hammond, Bo Xu

gb.hammond@louisville.edu (G.B.H.)
bo.xu@dhu.edu.cn (B.X.)

HIGHLIGHTS

A quantitative model for counterion effects was introduced

'Transition State Expansion' was used to describes how the size of a counterion affects the kinetics

Han et al., iScience *23*, 101593 October 23, 2020
https://doi.org/10.1016/j.isci.2020.101593

iScience

CellPress
OPEN ACCESS

Article

Transition-State Expansion: A Quantitative Model for Counterion Effects in Ionic Reactions

Junbin Han,[1] Zhichao Lu,[1] Gerald B. Hammond,[1,3,*] and Bo Xu[2,*]

SUMMARY

Ionic reactions are the most common reactions used in chemical synthesis. In relatively low dielectric constant solvents (e.g., dichloromethane, toluene), ions usually exist as ion pairs. Despite the importance of counterions, a quantitative description of how the paired 'counterion' affects the reaction kinetic is still elusive. We introduce a general and quantitative model, namely transition-state expansion (TSE), that describes how the size of a counterion affects the transition-state structure and the kinetics of an ionic reaction. This model could rationalize the counterion effects in nucleophilic substitutions and gold-catalyzed enyne cycloisomerizations.

INTRODUCTION

Chemical synthesis plays a vital role in pharmaceuticals, materials, agrochemicals, and many other related fields. Ionic reactions are the most common reactions in chemical synthesis (Dugger et al., 2005). According to a comprehensive survey of Good Manufacturing Practice (GMP) bulk reactions run in research facilities between 1985 and 2002 (Dugger et al., 2005), more than 68% of all C-C bond formations are ionic reactions. Examples of ionic reactions include nucleophilic substitutions (S_N), β-eliminations (E_2), enolate-based reactions (e.g., Aldol, Mannich reactions), Friedel-Crafts reactions, and many transition metal-catalyzed reactions (e.g., cationic gold catalysis). The role of counterion and ion pairing in organic reactions and transition metal-catalyzed transformations has been extensively investigated (Macchioni, 2005; Riddlestone et al., 2018; Chen and Lancaster, 2013). However, a quantitative description of how the paired 'counterion' affects the reaction kinetic is still elusive. The selection of counterions in synthesis is still empirical and relies heavily on a trial-and-error approach.

In an ionic reaction, the solvent plays a crucial role in the existing state of ions. If solvents of high dielectric constant (e.g., dimethyl sulphoxide [DMSO], water) are used, the ions are often fully dissociated and solvated. In this case, the counterion will be far away from the reaction center, and the counterion effect should be small. In a solvent of relatively low dielectric constant such as dichloromethane and toluene, ionic pairs may be the dominant species (Macchioni, 2005). In this case, the counterion will be close to the reaction center, and the counterion may have a significant effect on the reactivity. Although there was much empirical information on the counterion effect on individual ion reactions, to the best of our knowledge, there is no general quantitative description of how much ion pairing will affect an ionic reaction. In most theoretical studies of ionic reactions, counterions are simply ignored (Macchioni, 2005). Herein, we introduce a general and quantitative model on how sizes of counterions affect the transition-state structure and the kinetics of ionic reactions.

RESULTS

In a simplified representation of an ion reaction (Scheme 1A), a 'free' ion (A^-) reacts with reactants (RCT) to give the product via transition state (**TS-0**). Because **TS-0** includes both A^- and the reactants, **TS-0** could be bigger than A^- itself. We name this phenomenon '*transition-state expansion*' (TSE). As we discussed earlier, in a solvent of relatively low dielectric constant such as dichloromethane, ionic pairs may be the dominant species (Macchioni, 2005). The reaction of corresponding ion pair – [$A^- C^+$] will go through transition states **TS-1** (when the counterion C_1^+ is small) or **TS-2** (when the counterion C_2^+ is big), both of which are also ion pairs (Schemes 1B and 1C). Because **TS-1** and **TS-2** include both A^- and the reactants (RCT), **TS-1** and **TS-2** will also be bigger than the original ion pair ($A^- C^+$) (*TSE*). In other words, the distance between the center of positive charge and the center of negative charge will be longer ($r_1+\delta$ vs. r_1) if we assume ions are hard spheres. According to Coulomb's law, additional energy will be needed to overcome the

[1]Department of Chemistry, University of Louisville, Louisville, KY 40292, USA

[2]College of Chemistry, Chemical Engineering and Biotechnology, Donghua University, Shanghai 201620, China

[3]Lead Contact

*Correspondence: gb.hammond@louisville.edu (G.B.H.), bo.xu@dhu.edu.cn (B.X.)

https://doi.org/10.1016/j.isci.2020.101593

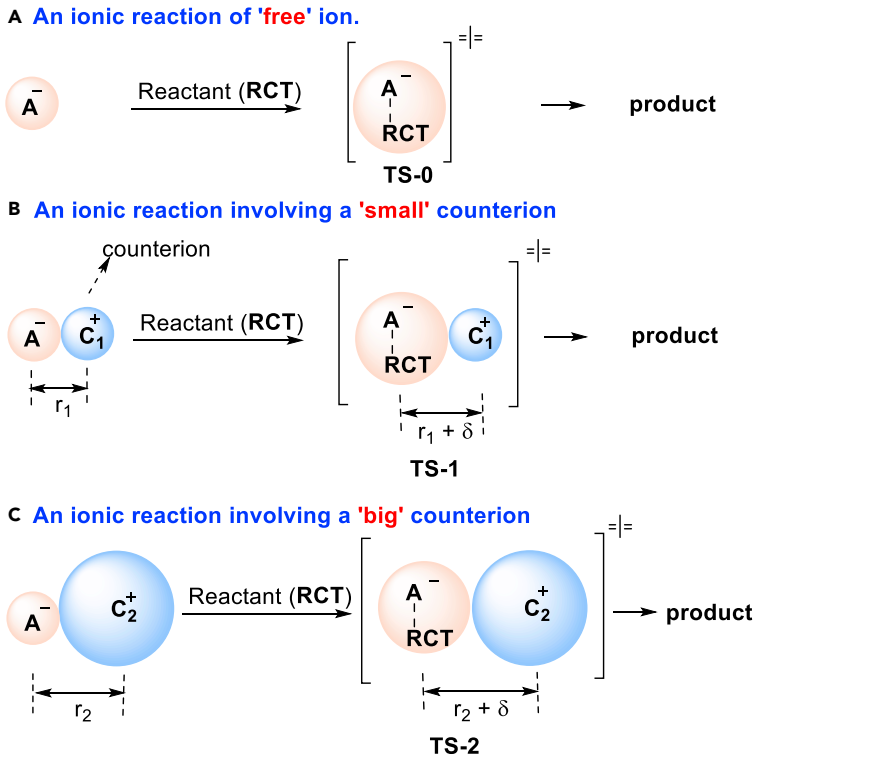

Scheme 1. Concept of Transition-State Expansion

attraction between cation and anion to reach transition states **TS-1** and **TS-2**. Also, according to Coulomb's law, the relationship between potential energy (E) and distance (r) is not linear (Scheme 1D). The energy needed to expand an ionic pair the same distance (ε) decreases significantly over distance r ($\Delta E_2 < \Delta E_1$). In other words, for **TS-2**, the energy required to overcome the Coulombic attraction will be smaller than that of **TS-1**. It should be noted that the ion pair ($A^- C^+$) can be a catalyst, reagent, or an intermediate.

We assume that all ion pairs and corresponding transition-state structures (**TS-1** or **TS-2**) can be treated as structureless hard balls. The rate constants (k_1 and k_2) for the reaction in Scheme 1 can be expressed as

Equation 2 (Eyring equation, where k_B is the Boltzmann constant and h is the Planck constant). Based on the above assumption, the activation energy difference between **TS-1** and **TS-2** will only be affected by the electrostatic component of the activation energies ($\Delta^{\ddagger}H_2^o - \Delta^{\ddagger}H_1^o$) (see Equation 5), which can be calculated from Coulomb's law (Equation 1). Other components of the activation energy, such as bond formation and bond rupture in the transition state, or change of solvation, are not influenced by the counterion. Based on those assumptions, the effect of the counterion ions [ln (k_2/k_1)] on the kinetics can be described by Equation 6. In Equation 6, there is a linear relationship between $\ln(k_2/k_1)$ and $\left[\left(\frac{1}{r_2}-\frac{1}{r_2+\delta}\right)-\left(\frac{1}{r_1}-\frac{1}{r_1+\delta}\right)\right]$ However, the TSE factor (δ) cannot be determined easily, so we cannot use this equation to verify our model. Because δ will be small compared to r_1 and r_2, then $\frac{1}{r_1}-\frac{1}{r_1+\delta}$ can be simplified as $-\frac{d\left(\frac{1}{r_1}\right)}{dr_1}\delta$, and Equation 6 can be simplified as Equation 7. Both r_1 and r_2 can be estimated using computational chemistry methods (see section 4 of Supplemental Information for more details), and k_1 and k_2 can be determined experimentally. Therefore, we could use Equation 7 to verify our kinetic model. We expect this model is especially suitable for reactions whose activation energy is dominated by the enthalpic contribution.

$$\Delta E = \frac{q_1 q_2}{4\pi\varepsilon}\frac{1}{r} \quad \text{(Equation 1)}$$

$$k = \frac{k_B T}{h}\exp\left(\frac{\Delta^{\ddagger}S^o}{R}\right)\exp\left(-\frac{\Delta^{\ddagger}H^o}{RT}\right) \quad \text{(Equation 2)}$$

$$\frac{k_2}{k_1} = \exp\left(\frac{\Delta^{\ddagger}S_2^o - \Delta^{\ddagger}S_1^o}{R}\right)\exp\left(-\frac{\Delta^{\ddagger}H_2^o - \Delta^{\ddagger}H_1^o}{RT}\right) \quad \text{(Equation 3)}$$

$$\Delta^{\ddagger}S_2^o - \Delta^{\ddagger}S_1^o = 0 \quad \text{(Equation 4)}$$

$$\Delta^{\ddagger}H_2^o - \Delta^{\ddagger}H_1^o = \frac{q_1 q_2}{4\pi\varepsilon}\left[\left(\frac{1}{r_2+\delta}-\frac{1}{r_2}\right)-\left(\frac{1}{r_1+\delta}-\frac{1}{r_1}\right)\right] \quad \text{(Equation 5)}$$

$$\ln\left(\frac{k_2}{k_1}\right) = -\frac{q_1 q_2}{4\pi\varepsilon RT}\left[\left(\frac{1}{r_2}-\frac{1}{r_2+\delta}\right)-\left(\frac{1}{r_1}-\frac{1}{r_1+\delta}\right)\right] \quad \text{(Equation 6)}$$

$$\ln\left(\frac{k_2}{k_1}\right) = -\frac{q_1 q_2}{4\pi\varepsilon RT}\left(-\frac{d\left(\frac{1}{r_2}\right)}{dr_2}\delta + \frac{d\left(\frac{1}{r_1}\right)}{dr_1}\delta\right) = -\frac{q_1 q_2 \delta}{4\pi\varepsilon RT}\left(\frac{1}{r_1^2}-\frac{1}{r_2^2}\right) =$$

$$A\left(\frac{1}{r_1^2}-\frac{1}{(r_1+\Delta r)^2}\right),\ \Delta r = r_2 - r_1, A = -\frac{q_1 q_2 \delta}{4\pi\varepsilon RT} \quad \text{(Equation 7)}$$

The above analysis is based on the assumption that a counterion does not affect the core structure of the transition state. In reality, the charged counterion should be able to distort the core structure of TS. We chose to begin our analysis by selecting one of the most synthetically important and also better-studied reactions—the bimolecular nucleophilic substitution reaction (S_N2) (Mikosch et al., 2008) (Scheme 2). The transition state in an S_N2 reaction involves the well-known Walden inversion (**TS-A**), where the anionic species **TS-A** shows a linear arrangement (Cl-C-Cl). We assume **TS-A** should be bigger than the starting anion (Cl^-) (***TSE***). Mechanistic studies of S_N2 reactions that take into account the effects of ion pairing are comparatively few (Harder et al., 1995; Streitwieser et al. 1997, 2008; Chen et al., 2009; Streitwieser and Jayasree, 2007; Zheng et al., 2010; Westaway, 2011; Li et al., 2015; Laloo et al., 2016).

TS-B is our hypothetical transition state for an S_N2 reaction with a contact ion pair. **TS-B** should have similar geometry to **TS-A**, but with the counterion arranged equidistantly to minimize Coulombic potential energy (Scheme 2B). Due to the TSE,' the distance between the center of positive charge and the center of negative charge will be longer than the starting ion pair. According to Coulomb's law (Equation 1), compared to the reaction using a free ion (**TS-A**), additional energy will be needed to overcome the attraction between cation and anion to reach the transition state **TS-B**. The transition state obtained by quantum chemistry calculations (**TS-C**) (Scheme 2C) is similar to our hypothetical transition state **TS-B**. However, we can see that the geometry of **TS-C** is not the same as **TS-A**; the most noticeable change is that Cl-C-Cl is no longer linear due to the attraction to the counterion (NMe_4^+). This bent or distorted transition state **TS-C** will be higher in energy than its linear counterpart **TS-A**. The energy difference can be obtained by DFT calculations: energy of **TS-C** (without a counterion) is higher than that of **TS-A**. A smaller counterion (e.g., Na^+) will induce even more distortion.

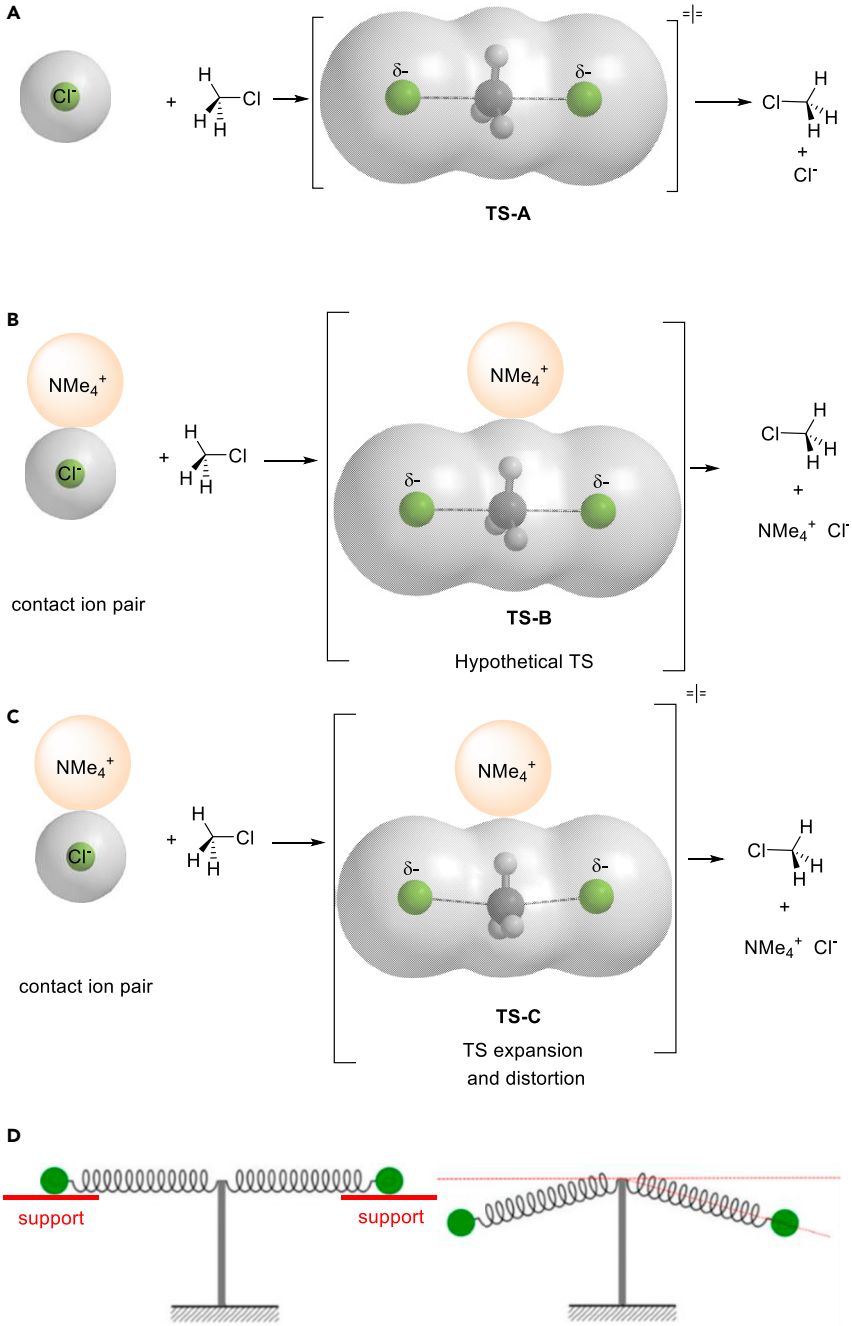

Scheme 2. Analysis of Nucleophilic Reactions Using the Concept of Transition-State Expansion

(A) The transition state in an S_N2 reaction when the counter is ignored.

(B) The hypothetical transition state for an S_N2 reaction with a contact ion pair.

(C) Calculated transition state for an S_N2 reaction with a contact ion pair.

(D) A ball/spring model in the gravitational field as an analogy.

Therefore, the total activation energy difference caused by a paired counterion (energy difference between **TS-A** and **TS-C**) will be the sum of two terms: ***expansion energy*** and ***distortion energy***. Dealing with two energy terms could be a complicated task. We hypothesize that **TS-C** and **TS-B** have very similar potential energies because—from a molecular mechanics point of view (bonds are considered springs)—the bending of two chlorine atoms brings the center of the negative change nearer to the counterion (center of positive charge). This effect reduces the Coulombic potential energy, which in turn is converted into

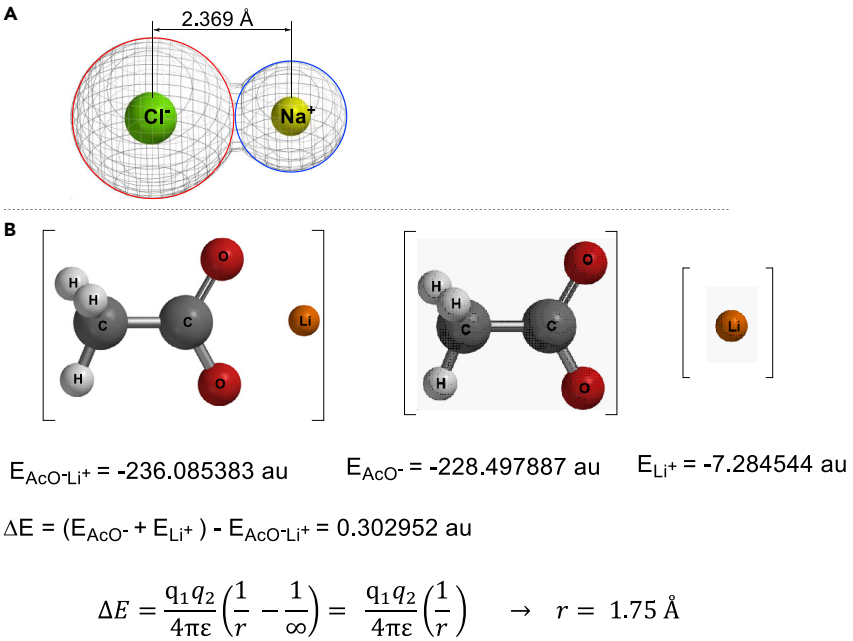

Figure 1. Equilibrium Geometry and Energies of AcO^-Li^+ Ion Pair and Individual Ions

potential energy caused by the bent of C-Cl bond (distortion energy). We can use the mechanics of a ball/spring model in a gravitational field as an analogy (Scheme 2D). In this model, first, we attach two balls to each end of the spring, then we take away the supports; the balls will go down because of gravity, but the energy of the whole system (balls plus spring) will remain the same because the gravitational potential energy will be converted into the elastic potential energy of the springs. In our ball/spring model, the gravity is analogous to the Coulombic attraction between a counterion and **TS-C,** and the spring is analogous to the C-Cl bond. This assumption significantly simplifies our calculations on the influence of different counterions on the activation energy because we only need to take into consideration the expansion energy. This assumption will make it possible to give a general model for counterion effects.

Determination of Charge Separation in an Ion Pair

To verify the kinetic model using Equation 7, we need quantitative information about the distance between cation and anion and the relative ion radii to establish the correlation between the reactivity of ionic reaction and the size of ions. Although both atoms and ions do not have sharp boundaries, they are sometimes treated as if they were hard spheres with radii such that the sum of ionic radii of the cation and anion gives the distance between the ions in a crystal lattice. The distance between two ions in an ionic crystal can be determined by X-ray crystallography (Shannon, 1976). However, although X-ray crystallography gives the distance between ions, it does not indicate where the boundary is between those ions, so it does not directly give ionic radii. However, the distance obtained from X-ray crystallography (solid state) is not necessarily the distance in the solution phase (ion pair). Spectroscopic methods and dynamic simulations have been proposed and used to quantify average interionic distances in solution (Correa and Cavallo, 2006; Zuccaccia et al., 2001; Macchioni et al., 2003). Furthermore, these data from X-ray crystallography and spectroscopic methods are limited; usually, only data for specific ions are available. To get a simple, general, and reliable method to estimate the distance between cation and anion in an ion pair, we used a computational chemistry method. All calculations were conducted using DFT B3LYP/6-31G* (gas phase). For ionic pairs with symmetric ions (e.g., chloride, BF_4^-), it is simple to determine the center of the cation and anion, so it is easy to determine the distance between cation and anion based on the ion pair's equilibrium geometry (Figure 1A). For example, the distance between Na^+ and Cl^- is 2.369 Å (Figure 1A). The direct method described above is simple to use. However, it is challenging to apply to ion pairs that contain unsymmetrical ions (e.g., AcO^-Li^+) because it is difficult to identify the center of the ions. In this case, we used the energy method (Figure 1B). We can calculate energies of AcO^-Li^+ ion pair and individual ions (AcO^- and Li^+) at their equilibrium geometries. ΔE will be the Coulombic potential energy caused by

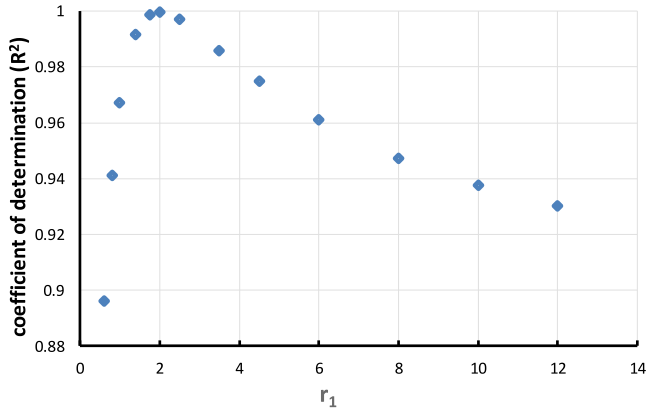

Figure 2. The Relationship between the Coefficient of Determination (R^2) of LSR Fitting and r_1

ion pairing; according to Coulomb's law, we can calculate r (distance) (Figure 1A). For most ion pairs, the two methods (direct and energy) give similar results; for example, for Na^+Cl^- ion pair, the direct method gives 2.37 Å, and the energy method gives 2.34 Å.

Kinetic Studies of Model Ionic Reactions

The first model of ionic reactions that we studied was the nucleophilic substitution reaction in both of its variances, S_N2, and S_N1. We began our experimental investigation with a typical S_N2 reaction, namely, the substitution of bromide by acetate in *n*-octyl bromide (Figure 3). The solvent we used was acetic acid because all the metal acetate salts studied had good solubility in this solvent and also because acetic acid has a low dielectric constant (ε = 6.15) and low solvation power. These metal acetates exist as non-dissociated ion pairs in this solvent (Jones and Griswold, 1954; El-Sherbini, 1996). We measured k_1 ($M^+ = Li^+$) and k_n ($M^+ = Na^+, K^+, Cs^+, Me_4N^+, Bu_4N^+$) and found that the reaction rate increased significantly with an increase in the size of the counterion (relative rates ranged from 1.0 to 28.5).

In theory, we could use Equation 7 to describe the counterion effects. Although r_1 (the charge separation in Li^+ OAc^-) in Equation 7 could be calculated from Figure 1 *via* Coulombic energy in a vacuum, in the reaction mixture, r_1 may be influenced by factors such as solvation and temperature, so it cannot be easily determined with great certainty. To simplify the calculation, we did linear least-squares regression (LSR) fitting using eq-7 for various possible r_1 (from 0.5 Å to 12 Å). In other words, we tried to find the 'best' r_1, which leads to the smallest fitting error using Equation 7. The XY scattering graph between the coefficient of determination (R^2) of LSR fitting vs. r_1 was shown in Figure 2. The optimal r_1 is between 1.70 Å and 2.1 Å. This value of r_1 is consistent with our calculation based on Coulombic energy in a vacuum (r_1 = 1.75 Å, Figure 1). When r_1 is determined, we found an excellent linear relationship using Equation 7.

From the report by Bordwell et al (Olmstead and Bordwell, 1980), metal acetates will exist as dissociated ions in a solvent of high dielectric constant like DMSO (ε = 46.7). As predicted by our model, the reactions of dissociated ions will have a small counterion effect. When we switched to DMSO as the solvent, the counterion effect became minimal indeed (range of k_n/k_1 = 0.7 to 1.2, Figure 4A).

In S_N1 reactions, counterions are not directly involved in the rate-determining step (carbon cation formation); we expect the counterion effect will be small. Our experimental results confirmed this expectation. We chose a typical S_N1 reaction—the reaction of adamantyl bromide with metal acetates. This S_N1 reaction was still fast when bigger counterion ions ($Na^+ < K^+ < Cs^+ < Me_4N^+ < Bu_4N^+$) were used, but the counterion effect was small (range of k_n/k_1 = 1.0 to 1.9, Figure 4B).

In the paragraphs above, we investigated two very typical S_N1 and S_N2 reactions, but not all S_N reactions are either S_N1 or S_N2. A case in point is the reaction of benzyl bromide with nucleophiles. We found that our quantitative study of counterion effects can also serve as a diagnostic tool: if the counterion effect is significant (k_n/k_1 close to a typical S_N2 reaction), then the reaction will have a strong S_N2 character. If the counterion effect is weak, the reaction will have a strong S_N1 character. Indeed, we proved that this was the case experimentally. When we

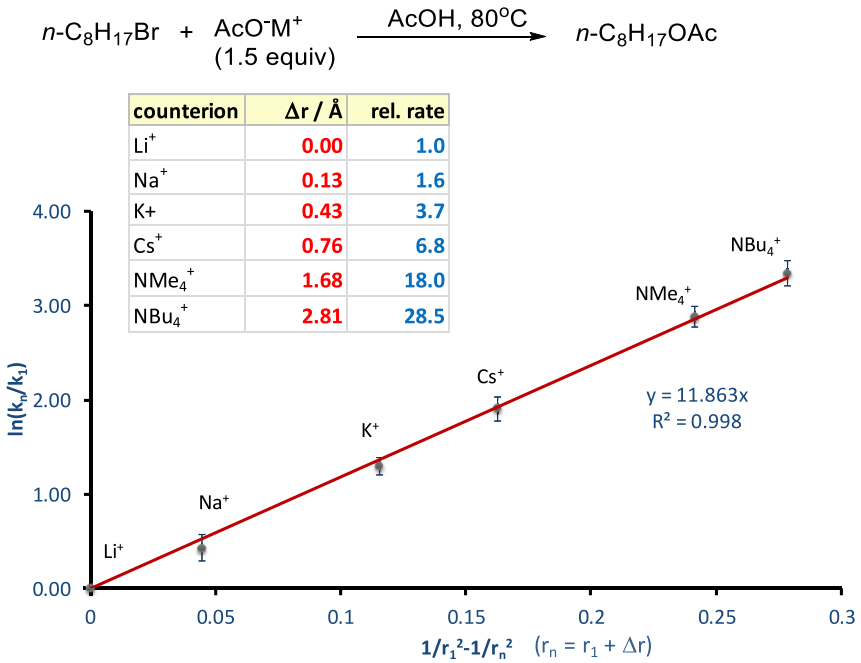

Figure 3. Description of S_N2 Reaction Using Equation 7 (r_1 = 1.75 Angstrom).

investigated the counterion effect in the reaction of benzyl bromide with metal acetates, we found that their kinetic effects were closer to the reaction in Figure 4C. Therefore, the mechanism of this reaction still possesses a stronger S_N2 character, but an S_N1 mechanism may operate at the same time.

It also should be pointed out that in many ionic reactions, especially in transition metal catalysis, multiple equilibria and several reactive intermediates might be involved in the catalytic cycle. Therefore, detailed mechanisms are challenging to establish, and in many cases, the rate-determining step may not begin with a simple M^+A^- ion itself, as shown in Scheme 1. For example, in cationic metal catalysis, a cationic metal may form a p or s complex with one reactant (RCT) first, and the rate-determining step may be the rearrangement of this complex without the involvement of a second reactant (Scheme 3). In the transition state, bond formation and bond rupture (in both cases, there will be bond elongation) will occur, causing a possible increase in the size (or charge separation between the centers of negative charge and positive charge) of the transition-state structure. It also should be noted that a counterion can be either a pure spectator or directly involved in the corresponding transition state.

Although most people would consider nucleophilic substitutions (e.g., S_N2) and gold-catalyzed enyne cycloisomerizations to be very different reactions, we have been able to explain their counterion effects using the similar treatment of the nucleophilic substitution (Figure 6). Unlike nucleophilic substitutions, gold-catalyzed reactions have a more complex mechanism, and the rate-determining step is often not clear. As a result, we could not calculate the r1 based on the structure of the transition state. Therefore, the determination of r_1 is not straightforward. However, we still could estimate r_1 based on the kinetic data similar to we did in S_N2 reactions. First, we did linear LSR fitting of Equation 7 for various possible r_1 (from 1.0 Å to 12 Å). The XY scattering graph between the coefficient of determination (R^2) of LSR fitting vs. r_1 was shown in Figure 5. The optimal r_1 is around 3.0 Å, which is reasonable for typical ionic gold complexes. To estimate the distance between cation and anion in a gold complex, we did the geometry optimization of one of the simplest cationic gold complexes (Me_3P-$Au^+BF_4^-$) using Gaussian 09 (see Supplemental Information section 4.3); the distance between Au and B atom is around 3.1 Å. It is generally accepted that the bond between Au and OTf in L-Au-OTf is not ionic, and our model is for ionic specie. As a result, although we measured the kinetic data for OTf-based reactions, we did not use it in our model (Equation 7).

Our model can also explain many isolated literature observations of transition metal-catalyzed reactions. Although quantitative kinetic data are not available in those literature reports, their findings consistently showed

A 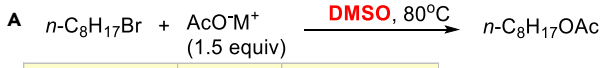

counterion	Δr / Å	rel. rate
Li^+	0.00	1.0
Na^+	0.13	0.7
K^+	0.43	0.9
Cs^+	0.76	1.1
NMe_4^+	1.68	1.2
NBu_4^+	2.81	1.0

B 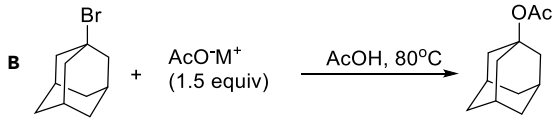

counterion	Δr / Å	rel. rate
Li^+	0.00	1.00
Na^+	0.13	1.10
K^+	0.43	1.32
Cs^+	0.76	1.90
NBu_4^+	2.81	1.96

C 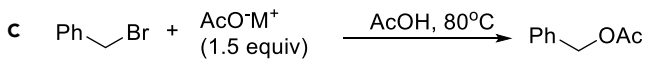

counterion	Δr / Å	rel. rate
Li^+	0.00	1.0
Na^+	0.13	1.1
K^+	0.43	2.5
Cs^+	0.76	3.2
NMe_4^+	1.68	7.1
NBu_4^+	2.81	7.3

Figure 4. Nucleophilic Substitution Reactions in Various Solvents

that larger counterions produce faster reaction rates. Selected examples include the copper-catalyzed Diels-Alder reaction (Scheme 4A) (Evans et al., 1999), the palladium-catalyzed CO/styrene copolymerization (Scheme 4B) (Macchioni et al., 1999), the rhodium-catalyzed additions of boronic acid to an aldehyde (Scheme 4C) (Moreau et al., 2001), and the iridium catalyzed hydrogenation of alkenes (Scheme 4D) (Smidt et al., 2004).

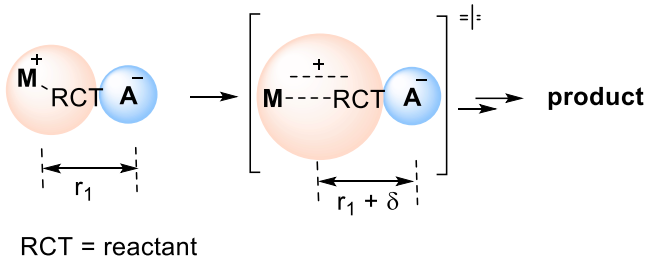

Scheme 3. Transition-State Expansion in a Rearrangement Step

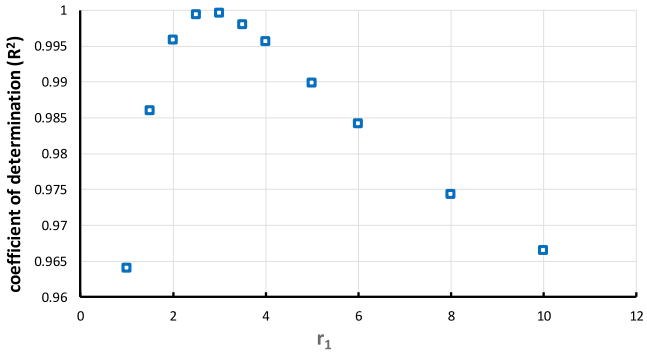

Figure 5. The Relationship between the Coefficient of Determination (R^2) of LSR Fitting and r_1 in the Gold-Catalyzed Enyne Cycloisomerization

We hypothesize that the counterion has a limited influence on the structures of the transition state in most cases. However, the above statement does have an exception. The interaction between a pairing counterion (X^-) and the corresponding transition structure is a long-range electrostatic attraction, which is usually relatively weak. While the long-range electrostatic attraction of a counterion may exhibit limited interaction with most atoms or groups, if the transition-state intermediate contains an active proton (e.g., O-H^{d+}), which has the smallest mass and is highly charged, then a counterion may have a significant impact (Scheme 5) via proton shuttling (Bandini et al., 2012). In these cases, the ability of a counterion to mediate the proton transfer (hydrogen bonding basicity) may play an important role. Indeed, in our previous investigation on the counterion effects on the gold-catalyzed reaction, we found that this was indeed the case (Lu et al., 2017).

Conclusion

In summary, we have postulated a general model, namely 'transition-state expansion,' to describe the influence of the counterion on the kinetics of ionic reactions. This model describes how the size of a counterion affects the transition-state structure and the kinetics of an ionic reaction in a quantitative manner. Further implications and applications of this model are under investigation in our laboratory.

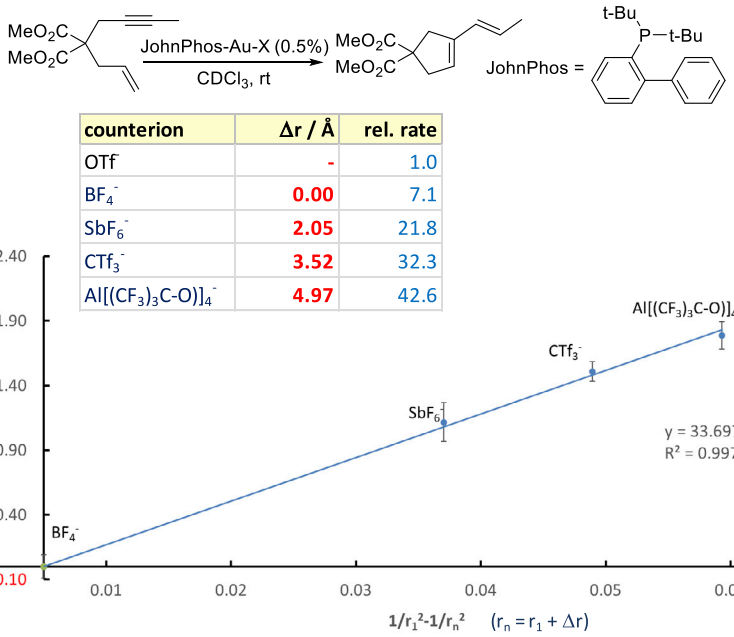

Figure 6. Cationic Gold-Catalyzed Cycloisomerization of 1,6-enyne (Calculations Are Based on r_1 = 3.0 Å, Data for OTf^- Was Not Used).

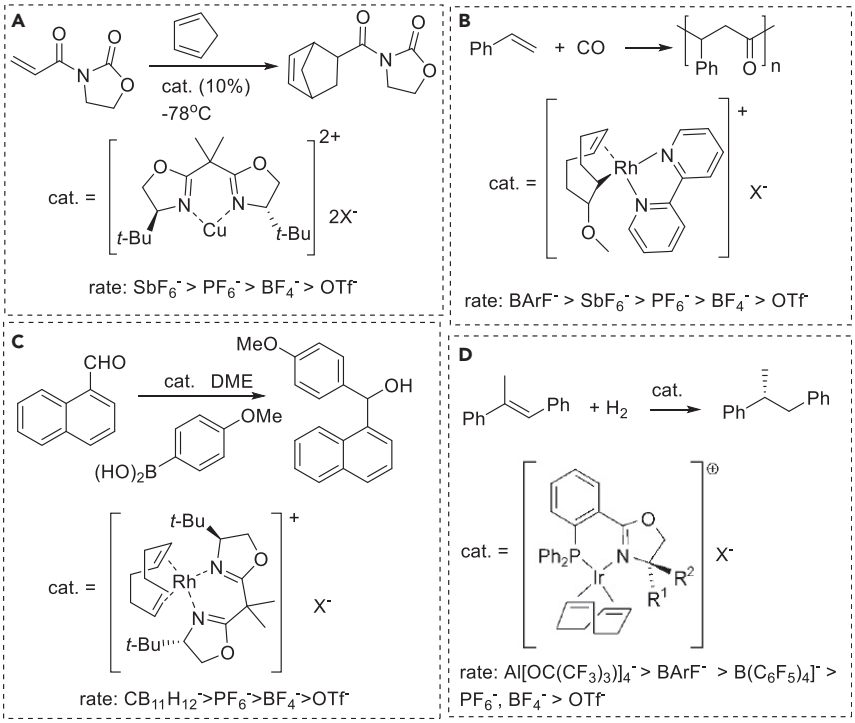

Scheme 4. Selected Literature Examples Showing Primary Counterion Effects

Limitations of the Study

Among many ionic reactions, only nucleophilic substitutions and cationic gold-catalyzed reactions were studied.

DATA AND CODE AVAILABILITY

Procedure for experiments and characterization data for products are available in Supplemental Information.

METHODS

All methods can be found in the accompanying Transparent Methods supplemental file.

SUPPLEMENTAL INFORMATION

Supplemental Information can be found online at https://doi.org/10.1016/j.isci.2020.101593.

ACKNOWLEDGMENTS

We are grateful to the National Science Foundation (CHE-1855972) for financial support. B.X. is grateful to the National Science Foundation of China (NSFC-21672035, NSFC-21871046) for financial support.

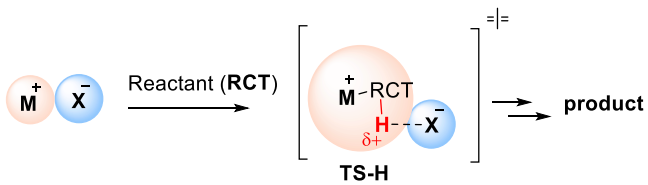

Scheme 5. A Transition State Involves an Active Proton Transfer

AUTHOR CONTRIBUTIONS

Conceptualization, G.B.H. and X.B.; Investigation, J.H. and Z.L.; Writing – Orignal Draft, G.B.H. and X.B.; Writing – Review & Editing, G.B.H. and X.B.

DECLARATION OF INTERESTS

The authors declare no competing interests.

Received: April 4, 2020
Revised: August 3, 2020
Accepted: September 17, 2020
Published: October 23, 2020

REFERENCES

Bandini, M., Bottoni, A., Chiarucci, M., Cera, G., and Miscione, G.P. (2012). Mechanistic insights into enantioselective gold-catalyzed allylation of indoles with alcohols: the counterion effect. J. Am. Chem. Soc. *134*, 20690–20700.

Chen, E.Y.X., and Lancaster, S.J. (2013). 1.24 - weakly coordinating anions: highly fluorinated borates. In Comprehensive Inorganic Chemistry II, Second Edition, J. Reedijk and K. Poeppelmeier, eds. (Elsevier), pp. 707–754.

Chen, X., Regan, C.K., Craig, S.L., Krenske, E.H., Houk, K.N., Jorgensen, W.L., and Brauman, J.I. (2009). Steric and solvation effects in ionic S_N2 reactions. J. Am. Chem. Soc. *131*, 16162–16170.

Correa, A., and Cavallo, L. (2006). Dynamic properties of metallocenium ion pairs in solution by atomistic simulations. J. Am. Chem. Soc. *128*, 10952–10959.

Dugger, R.W., Ragan, J.A., and Ripin, D.H.B. (2005). Survey of GMP bulk reactions run in a research facility between 1985 and 2002, *Org.* Process. Res. Dev. *9*, 253–258.

El-Sherbini, E.E.F. (1996). Electrical conductance studies of alkali metal acetates in anhydrous acetic acid solutions, *Egypt.* J. Chem. *39*, 205–213.

Evans, D.A., Miller, S.J., Lectka, T., and von Matt, P. (1999). Chiral bis(oxazoline)copper(II) complexes as lewis acid catalysts for the enantioselective Diels−Alder reaction. J. Am. Chem. Soc. *121*, 7559–7573.

Harder, S., Streitwieser, A., Petty, J.T., and von Schleyer, P. (1995). Ion pair S_N2 reactions. Theoretical study of inversion and retention mechanisms. J. Am. Chem. Soc. *117*, 3253–3259.

Jones, M.M., and Griswold, E. (1954). Conductances of some salts and ion-pair equilibria in acetic acid at 30°. J. Am. Chem. Soc. *76*, 3247–3249.

Laloo, J.Z.A., Rhyman, L., Ramasami, P., Bickelhaupt, F.M., and de Cozar, A. (2016). Ion-pair S_N2 substitution: activation strain analyses of counter-ion and solvent effects. Chem. Eur. J. *22*, 4431–4439.

Li, Q.-G., Xu, K., and Ren, Y. (2015). Origin of enhanced reactivity of a microsolvated nucleophile in ion pair S_N2 reactions: the cases of sodium p-nitrophenoxide with halomethanes in acetone. J. Phys. Chem. A *119*, 3878–3886.

Lu, Z., Han, J., Okoromoba, O.E., Shimizu, N., Amii, H., Tormena, C.F., Hammond, G.B., and Xu, B. (2017). Predicting counterion effects using a gold affinity index and a hydrogen bonding basicity index. Org. Lett. *19*, 5848–5851.

Macchioni, A. (2005). Ion pairing in transition-metal organometallic chemistry. Chem. Rev. *105*, 2039–2074.

Macchioni, A., Bellachioma, G., Cardaci, G., Travaglia, M., Zuccaccia, C., Milani, B., Corso, G., Zangrando, E., Mestroni, G., Carfagna, C., and Formica, M. (1999). Counterion effect on CO/styrene copolymerization catalyzed by cationic palladium(II) organometallic Complexes: an interionic structural and dynamic investigation based on NMR spectroscopy. Organometallics *18*, 3061–3069.

Macchioni, A., Magistrato, A., Orabona, I., Ruffo, F., Rothlisberger, U., and Zuccaccia, C. (2003). Direct observation of an equilibrium between two anion-cation orientations in olefin Pt(II) complex ion pairs by HOESY NMR spectroscopy. New J. Chem. *27*, 455–458.

Mikosch, J., Trippel, S., Eichhorn, C., Otto, R., Lourderaj, U., Zhang, J.X., Hase, W.L., Weidemüller, M., and Wester, R. (2008). Imaging nucleophilic substitution dynamics. Science *319*, 183–186.

Moreau, C., Hague, C., Weller, A.S., and Frost, C.G. (2001). Rhodium-catalysed aryl transfer to aldehydes: counterion effects with nitrogen containing ligands. Tetrahedron Lett. *42*, 6957–6960.

Olmstead, W.N., and Bordwell, F.G. (1980). Ion-pair association constants in dimethyl sulfoxide. J. Org. Chem. *45*, 3299–3305.

Riddlestone, I.M., Kraft, A., Schaefer, J., and Krossing, I. (2018). Taming the cationic beast: novel developments in the synthesis and application of weakly coordinating anions. Angew. Chem. Int. Ed. *57*, 13982–14024.

Shannon, R. (1976). Revised effective ionic radii and systematic studies of interatomic distances in halides and chalcogenides. Acta Crystallogr. A. *32*, 751–767.

Smidt, S.P., Zimmermann, N., Studer, M., and Pfaltz, A. (2004). Enantioselective hydrogenation of alkenes with iridium–PHOX catalysts: a kinetic study of anion effects. Chem. Eur. J. *10*, 4685–4693.

Streitwieser, A., Choy, G.S.-C., and Abu-Hasanayn, F. (1997). Theoretical study of ion pair S_N2 Reactions: ethyl vs methyl reactivities and extension to higher alkyls. J. Am. Chem. Soc. *119*, 5013–5019.

Streitwieser, A., and Jayasree, E.G. (2007). Theoretical study of the effect of coordinating solvent on ion pair S_N2 Reactions: the role of unsymmetrical transition structures. J. Org. Chem. *72*, 1785–1798.

Streitwieser, A., Jayasree, E.G., Hasanayn, F., and Leung, S.S.H. (2008). A theoretical study of S_N2' reactions of allylic halides: role of ion pairs. J. Org. Chem. *73*, 9426–9434.

Westaway, K.C. (2011). Nucleophilic aliphatic substitution. Org. React. Mech. 201–238.

Zheng, S., Xiong, Y., and Wang, J. (2010). Theoretical studies on identity S_N2 reactions of lithium halide and methyl halide: a microhydration model. J. Mol. Model. *16*, 1931–1937.

Zuccaccia, C., Bellachioma, G., Cardaci, G., and Macchioni, A. (2001). Solution structure investigation of Ru(II) complex ion Pairs: quantitative NOE measurements and determination of average interionic distances. J. Am. Chem. Soc. *123*, 11020–11028.

iScience, Volume *23*

Supplemental Information

Transition-State Expansion: A Quantitative Model for Counterion Effects in Ionic Reactions

Junbin Han, Zhichao Lu, Gerald B. Hammond, and Bo Xu

Transparent Methods

Section 1. General

^{1}H, ^{13}C, and ^{31}P NMR spectra were recorded at 400, 100, and 162 MHz, respectively, using $CDCl_3$ as a solvent. The chemical shifts are reported in δ (ppm) values relative to $CHCl_3$ (δ 7.26 ppm for ^{1}H NMR and δ 77.0 ppm for ^{13}C NMR) and $CFCl_3$ (δ 0 ppm for ^{19}F NMR), multiplicities are indicated by s (singlet), d (doublet), t (triplet), q (quartet), p (pentet), h (hextet), m (multiplet) and br (broad). Coupling constants, *J*, are reported in Hertz. All air and/or moisture-sensitive reactions were carried out under argon atmosphere. Solvents (tetrahydrofuran, ether, dichloromethane, and DMF) were chemically dried using a commercial solvent purification system. All other reagents and solvents were employed without further purification. The products were purified using a CombiFlash system or a regular glass column. TLC was developed on Merck silica gel 60 F254 aluminum sheets. $KCTf_3$ was purchased from Synquest Labs, $Ag^{+}[Al[(CF_3)_3C\text{-}O)]_4]^{-}$ was purchased from IoLiTec. All other chemicals like metal catalysts and ligands were purchased from Aldrich, Alfa Aesar, or Strem.

Section 2. General procedure for kinetic measurements

2.1 Monitoring of reactions using *in situ* NMR spectroscopy

When ^{1}H NMR was used to monitor the progress of a reaction, a solution of tetramethylsilane in $CDCl_3$ (sealed in a capillary tube) was used as an external standard for NMR integration. When ^{31}P NMR was used to monitor the progress of the reaction, 85% H_3PO_4 (sealed in a capillary tube) was used as an external standard for NMR integration. In some cases, 1,3,5-tri-*tert*-butylbenzene (internal standard) was used. The reactions were monitored with ^{1}H NMR (single pulse or 1 scan for fast reactions, 8 scans for slow reactions). Some NMR measurements were conducted using the NMR experiment array (a series of spectra measured at predetermined time intervals over a period of time by adjusting the pre-acquisition delay). NMR experiment array gives better precision for both concentration (*via* integrations) and reaction time because each measurement is conducted at almost identical shimming and temperature conditions. The concentrations of substrate and product were determined by relative integration to the t-butyl peak in the standard (tetramethylsilane or 1,3,5-tri-*tert*-butylbenzene).

2.2 Monitoring of reactions using *GC-MS.*

The model reaction was conducted in the presence of an internal standard (hexadecane or acetophenone). For analysis, 1-5 μL of the sample was taken from the reaction mixture and was diluted with a suitable solvent (e.g., hexane or ethyl acetate). The diluted solution was injected into a GC-MS using an autosampler. Each GC reading is the average of three runs. Typically three reactions under the same conditions were conducted in parallel.

Section 3. Synthesis of starting materials

Synthesis of gold complexes (L-AuCl). All gold complexes (L-AuCl) were synthesized using a slightly modified version of a literature method.(Nieto-Oberhuber et al., 2005) These complexes were prepared via the following general procedure:

Sodium tetrachloroaurate(III) dihydrate (1 mmol) was dissolved in water, and the orange solution was cooled in ice. To this solution, 2,2'-thiodiethanol (3 mmol) was slowly added (ca. 45 min) with stirring. A solution of the phosphine ligand (1 mmol) in EtOH (if the ligand could not be dissolved, more EtOH was used) was added dropwise to yield a white solid. The solid was filtered off, washed with water followed by EtOH, and ultimately dried in vacuum.

Preparation of cationic gold (L-Au$^+$X$^-$) stock solution. Standard stock solutions of cationic gold catalyst were made by weighing the L-Au(I)Cl complex into a vial and adding corresponding deuterated solvent, then 1.2 equiv of AgX was added, the vial was sonicated for 3-5 min at 5-10 ºC, then the vial was centrifuged, and the clear solution was transferred to a clean glass vial with a screw cap. The solution was kept in the freezer (-20 ºC) until it was used.

Section 4. Determination of the distance between cation and anion in an ion pair and radii of ions

We need quantitative information about the distance between cation and anion and the ion radii to establish the correlation between the reactivity of ionic reaction and the size of ions. Although neither atoms nor ions have sharp boundaries, they are sometimes treated as if they were hard spheres with radii such that the sum of ionic radii of the cation and anion gives the distance between the ions in a crystal lattice. The distance between two ions in an ionic crystal can be determined by X-ray crystallography (Shannon, 1976). However, although X-ray crystallography gives the distance between ions, it doesn't indicate where the boundary is between those ions, so it does not directly give ionic radii. But the distance obtained from X-ray crystallography (solid-state) is not necessarily the distance in the solution phase (ion pair); furthermore, data from X-ray crystallography are limited. Usually, only data for simple ions are available. In order to get a simple, general, and reliable method to estimate the distance between cation and anion in an ion pair, we used a computational chemistry method. All calculations were conducted using Spartan 16 (DFT B3LYP/6-31G* in the gas phase).

4.1 Calculation of distance between cation and anion.

Direct method. It is straightforward to build a model of ion-pair using commercial quantum chemistry software (e.g., Spartan 10 or GaussianView 5.0). For ionic ion pairs with symmetric ions (e.g., chloride, BF_4^-), it is simple to determine the center of the cation and anion, so it is easy to determine the distance between cation and anion based on the ion pair's equilibrium geometry (Figure S - 1). For example, the distance between Na^+ and Cl^- is 2.369 Å (Figure S - 1).

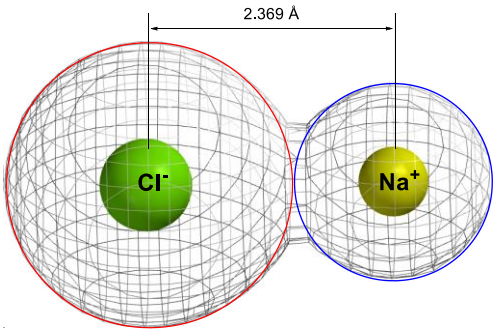

Figure S - 1. Equilibrium geometry of Na^+Cl^- ion pair, related to Figure 1a

Energy method. The direct method described above is simple to use. However, it is challenging to apply it to ion pairs that contain unsymmetrical ions (e.g., AcO^-Li^+) because it is difficult to identify the center of the ions. In this case, we use the energy method (Figure S - 2). We can calculate energies of AcO^-Li^+ ion pair and individual ions (AcO^- and Li^+) at their equilibrium geometries. ΔE will be the Coulombic potential energy caused by ion-pairing, according to Coulomb's law, we can calculate r (distance) (Figure S - 2).

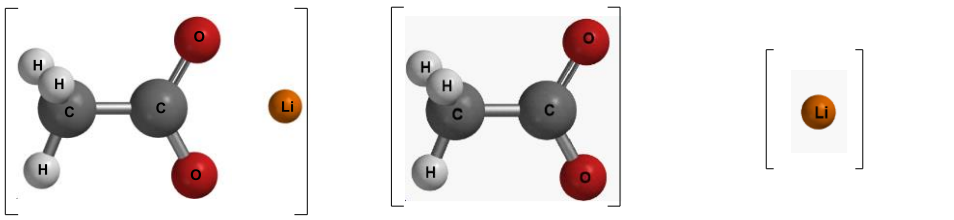

$E_{AcO-Li+}$ = -236.085383 au E_{AcO-} = -228.497887 au E_{Li+} = -7.284544 au

$\Delta E = (E_{AcO-} + E_{Li+}) - E_{AcO-Li+}$ = 0.302952 au

$$\Delta E = \frac{q_1 q_2}{4\pi\varepsilon}\frac{1}{r} \qquad \rightarrow \qquad r(distance) = \ 1.75\ A$$

Figure S - 2. Equilibrium geometry and energies of AcO^-Li^+ ion pair and individual ions, related to Figure 1b

For most ion pairs, the two methods (direct and energy) give similar results. For example, for Na^+Cl^- ion pair, the direct method gives 2.37 Å, and the energy method gives 2.34 Å.

4.2 Calculation of ion radius

Volume method. Now we can use the direct method and the energy method to calculate the distance between cation and anion. However, these methods do not indicate where the boundary is between those ions, so they do not directly give ionic radii. For the calculation of the ion radius, we will use the volume method. We can calculate the electron density surface for both the cation and anion, and then calculate the volume of cation and anion by

selecting an isoVal, which makes the surface to include 94.5% of electron density (Figure S - 3). Then based on the volume of ions, we can calculate their radii by assuming they are all spheres. The reason to use 94.5% of electron density to define the boundary of ions is the sum of radii of cation, and ion is very close to the calculated distance between anion and cation in the ion pair for most ion pairs (Figure S - 3). Based on the volume method, we calculated the radii for commonly used anions and cations (Table S - 1, Figure S - 4).

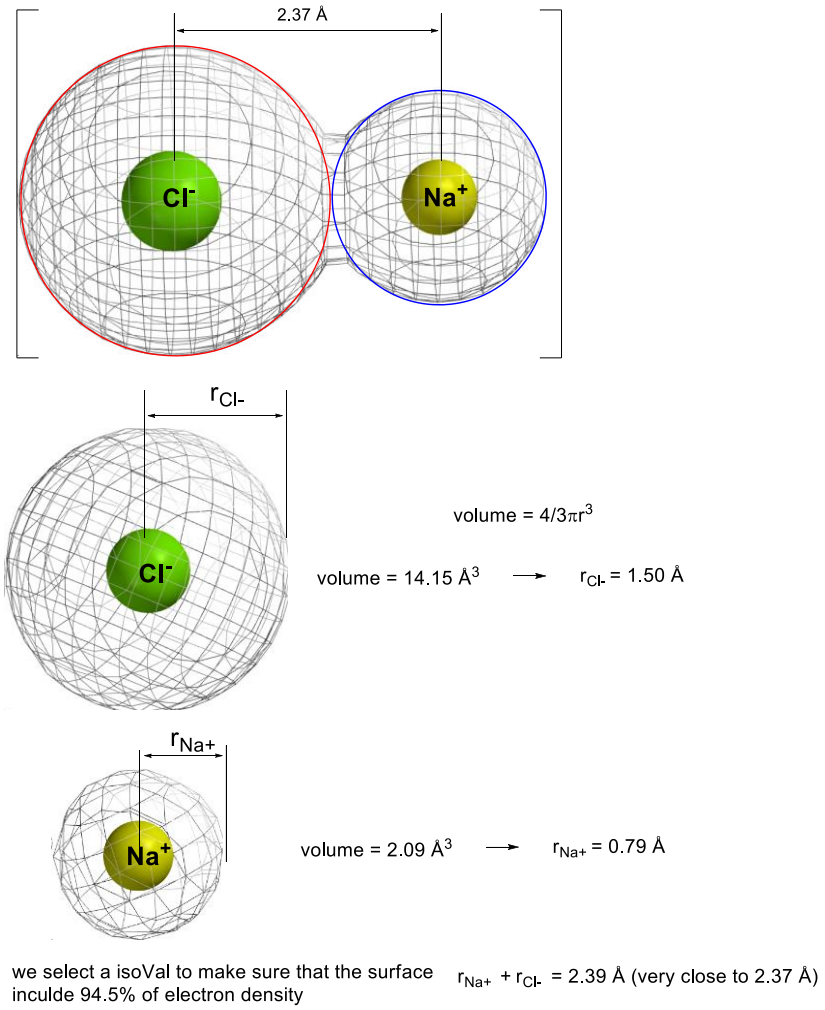

Figure S - 3. Volume method for calculation of ion radius, related to Figure 1b

Table S - 1. Calculation for the size of ions, related to Figure 1b

ions	volume Å^3	radius / Å	Δr^a / Å
anions			
BF_4^-	22.36	1.75	0.00
SbF_6^-	79.11	2.66	0.92
CTf_3^-	104.15	2.92	1.17
$Al[(CF_3)_3C\text{-}O)]_4^-$	244.00	3.88	2.13
cations			
Li^+	1.18	0.66	0.00
Na^+	2.09	0.79	0.13
K^+	5.38	1.09	0.43
Cs^+	12.01	1.42	0.76
NMe_4^+	53.41	2.34	1.68
NBu_4^+	175.02	3.47	2.81

[a] $\Delta r = r_n - r_1$, for anions, BF_4^- is used as reference (r_1), for cation, Li^+ is used as reference (r_1).

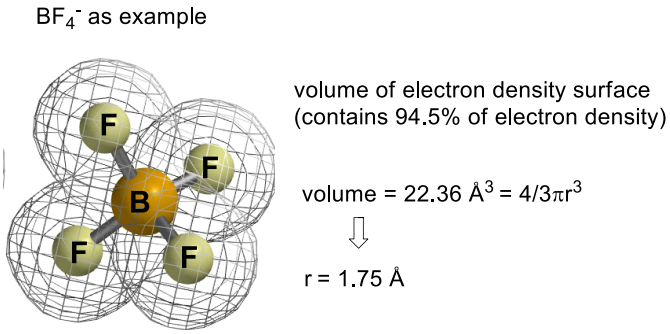

Figure S - 4. The calculation for the size of BF_4^- using the volume method, related to Figure 1

4.3 Estimation of the distance between cation and anion in gold complexes

To estimate the distance between cation and anion in a gold complex, we did the geometry optimization of one of the simplest cationic gold complex ($Me_3P\text{-}Au^+BF_4^-$) using Gaussian 09 (M. J. Frisch, 2016) (Figure S - 5). The distance between Au and B atom is around 3.1 Å.

Calculation Type = FREQ

Calculation Method = RB3LYP

Basis Set = GenECP

Charge = 0

Spin = Singlet

E(RB3LYP) = -1021.26713337 a.u.

RMS Gradient Norm = 0.00000424 a.u.

Imaginary Freq = 0

Dipole Moment = 15.3652 Debye

Point Group = C1

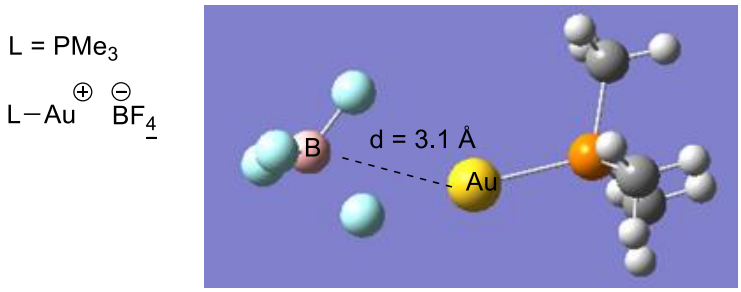

Figure S - 5. Geometry optimization of Me_3P-$Au^+BF_4^-$, related to Figure 6

Section 5. Initial reaction rate measurements and correlation with counterion size.

5.1 General procedure for initial reaction rate measurements.

The model reactions were conducted using prepared stock solutions and were monitored until their conversion reached up to 15%, following the general procedure for kinetic experiments using *in situ* NMR spectroscopy or GC-MS. Because in the initial period of the reaction, the kinetic curve appeared to be linear, we used the linear least-squares fit of the data to determine the slope (reaction rate V_o). The average initial rate (V_0) reported reflects an average of at least three kinetic runs. The concentration unit used is mM.

5.2 Nucleophilic substitution reactions (S_N)

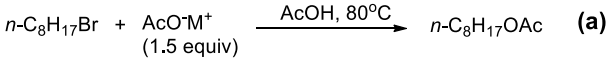

$M^+ = Li^+, Na^+, K^+, Cs^+, Me_4N^+, Bu_4N^+$

The standard solution of starting material was prepared by mixing 1-bromoalkane (3.6 mmol) and *n*-hexadecane (0.3 mmol, internal standard) in 7.2 mL acetic acid. Different metal acetate salts ($M^+ = Na^+$, K^+, Cs^+, Me_4N^+,

Bu_4N^+, each 1.6 mmol) were dissolved in 1.6 mL acetic acid, and 0.4 mL of a standard solution containing bromoalkane was added. The reaction mixture was stirred and heated to 80 °C. For analysis, 1-5 µL of the sample was taken from the reaction mixture and was diluted with a suitable solvent (e.g., hexane or ethyl acetate). The diluted solution was injected into a GC-MS using an autosampler. Each GC reading is the average of three runs. Typically three reactions under the same conditions were conducted in parallel. A typical measurement is shown in Figure S - 6, Table S - 2, Table S - 3.

Nucleophilic substitution of primary alkyl bromide in acetic acid

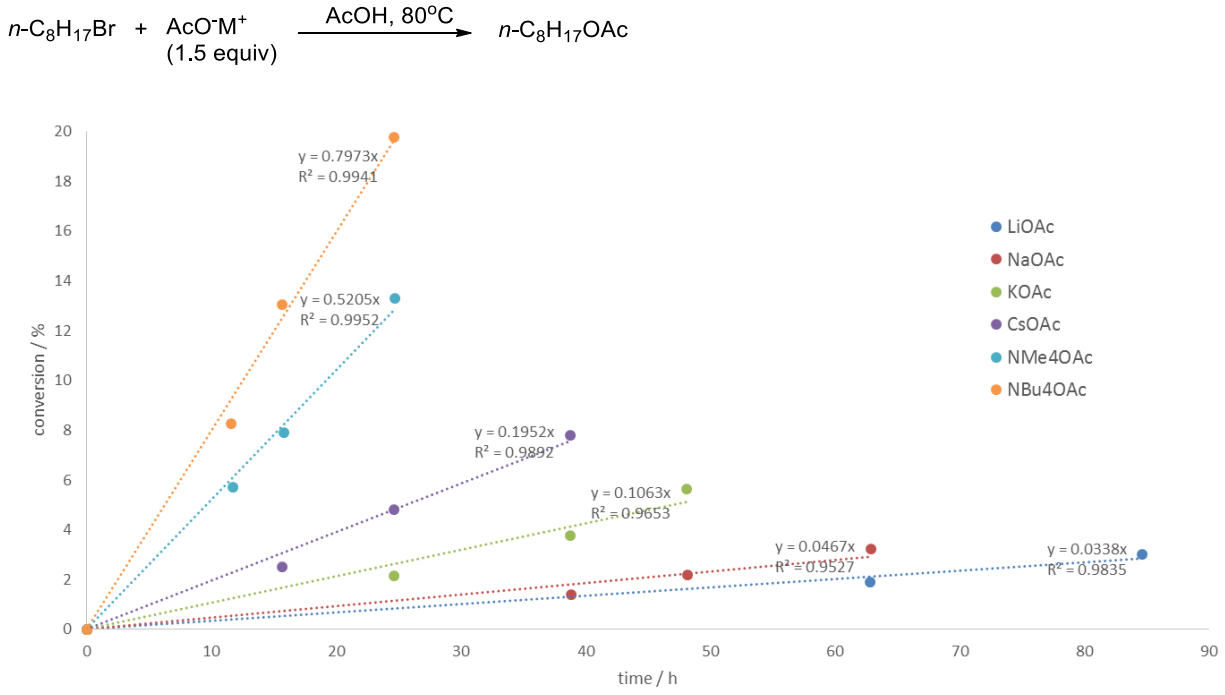

Figure S - 6. Determination of the initial reaction rate for the reaction of the *n*-$C_8H_{17}Br$ with metal acetate in acetic acid, related to Figure 3

Table S - 2. The initial reaction rate for the reaction of the *n*-$C_8H_{17}Br$ with metal acetate in acetic acid, related to Figure 3

cations	trial 1	trial 2	trial 3	trial 4	trial 5	trial 6	average relative initial reaction rate	average initial reaction rate ($mol \cdot L^{-1}h^{-1}$)	$\ln(k_n/k_1)$	standard deviation of $\ln(k_n/k_1)$
Li^+	1.00	1.00	1.00	1.00	1.00	1.00	1.00	0.017	0.00	0.00
Na^+	1.46	1.37	1.41	1.38	1.86	1.82	1.55	0.023	0.43	0.14
K+	3.50	3.33	3.59	3.48	4.14	4.03	3.68	0.056	1.30	0.09
Cs^+	6.09	6.02	6.46	6.32	7.95	7.84	6.78	0.102	1.91	0.13

NMe_4^+	16.93	15.52	17.53	17.06	20.57	20.29	17.98	0.262	2.88	0.11
NBu_4^+	26.90	23.96	28.73	25.43	34.37	31.79	28.53	0.405	3.34	0.14

Table S - 3. Correlation between size of counterions and the reactivity, related to Figure 3

Cations	Δr / Å	$r_1^2-r_n^2$	$\ln(k_n/k_1)$	standard deviation of $\ln(k_n/k_1)$
Li^+	0.00	0.00	0.00	0.00
Na^+	0.13	0.04	0.43	0.14
K^+	0.43	0.12	1.30	0.09
Cs^+	0.76	0.17	1.91	0.13
NMe_4^+	1.68	0.24	2.88	0.11
NBu_4^+	2.81	0.28	3.34	0.14

Nucleophilic substitution of benzyl bromide

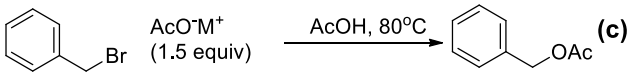

$M^+ = Li^+, Na^+, K^+, Cs^+, Me_4N^+, Bu_4N^+$

Table S - 4. The initial reaction rate for the reaction of BnBr with metal acetate in acetic acid, related to Figure 4c

Cations	trial 1	trial 2	trial 3	average relative initial reaction rate	average initial reaction rate ($mol \cdot L^{-1}h^{-1}$)	$\ln(k_n/k_1)$	standard deviation of $\ln(k_n/k_1)$
Li^+	1.00	1.00	1.00	1.00	0.013	0.00	0.00
Na^+	1.17	1.11	1.15	1.14	0.014	0.13	0.03
K^+	2.68	2.42	2.54	2.55	0.030	0.93	0.05
Cs^+	2.98	3.49	3.28	3.25	0.044	1.18	0.08
NMe_4^+	7.36	6.78	7.12	7.09	0.085	1.96	0.04
NBu_4^+	7.42	7.13	7.38	7.31	0.089	1.99	0.02

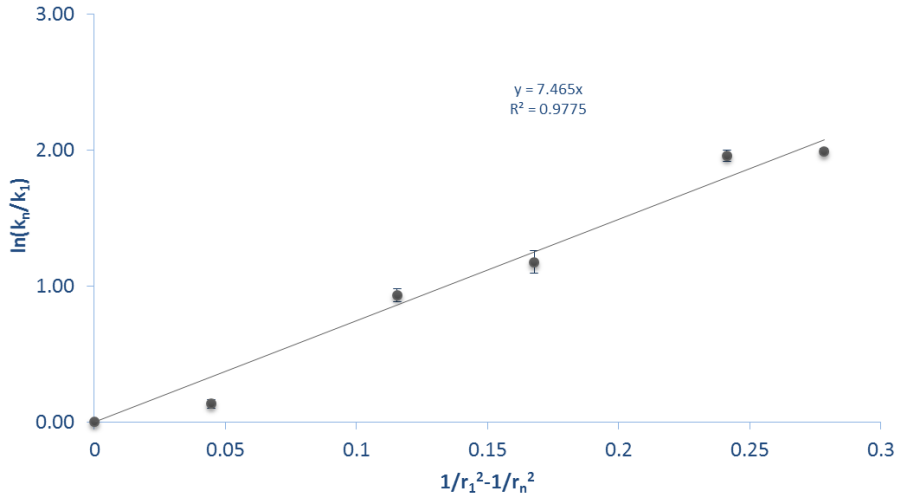

Figure S - 7. Counterion effect for nucleophilic substitution of benzyl bromide, related to Figure 4c

Nucleophilic substitution of primary alkyl bromide in DMSO

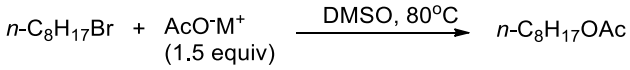

Table S - 5. The initial reaction rate for the reaction of *n*-C_8H_{17}Br with metal acetate in DMSO, related to Figure 4a

counterio	Δr / Å	rel. rate
Li^+	0.00	1.0
Na^+	0.13	0.7
K^+	0.43	0.9
Cs^+	0.76	1.1
NMe_4^+	1.68	1.2
NBu_4^+	2.81	1.0

Nucleophilic substitution of adamantyl bromide

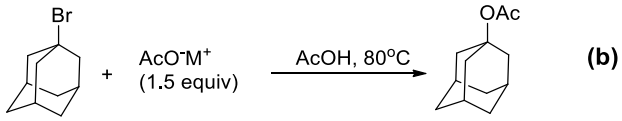

(b)

Table S - 6. The initial reaction rate for the reaction of adamantyl bromide with metal acetate in acetic acid, related to Figure 4b

counterion	Δr / Å	rel. rate
Li^+	0.00	1.00
Na^+	0.13	1.10
K^+	0.43	1.32
Cs^+	0.76	1.90
NBu_4^+	2.81	1.96

5.3 Initial reaction rate measurement for gold catalysis.

Preparation of cationic gold (L-Au^{+}X^{-}) stock solution. Standard stock solutions of cationic gold catalyst were made by weighing the L-Au(I)Cl complex into a vial and adding corresponding deuterated solvent, then 1.2 equiv of AgX was added, the vial was sonicated for 3-5 min at 5-10 °C, then the vial was centrifuged, and the clear solution was transferred to a clean glass vial with a screw cap. The solution was kept in the freezer (-20 °C) until it was used.

Following the general procedure for cationic gold-stock solution preparation, the substrate (1,6-enyne, 0.1 mmol in $CDCl_3$ 0.5 mL) and stock solutions containing gold(I) catalyst and the internal standard were added into a J-Young NMR tube protected from light. The reaction was kept at room temperature and was monitored until conversion reached 15% following the general procedure for kinetic experiments using *in situ* NMR spectroscopy. Because during the initial period of reaction, the kinetic curve appeared to be linear, we used the linear least-squares fit of the data to determine the slope (reaction rate V_o). The average initial rate (V_0) reported reflects an average of three kinetic runs. A representative plot of conversion versus time (h) is shown in Figure S - 8, Table S - 7, Table S - 8.

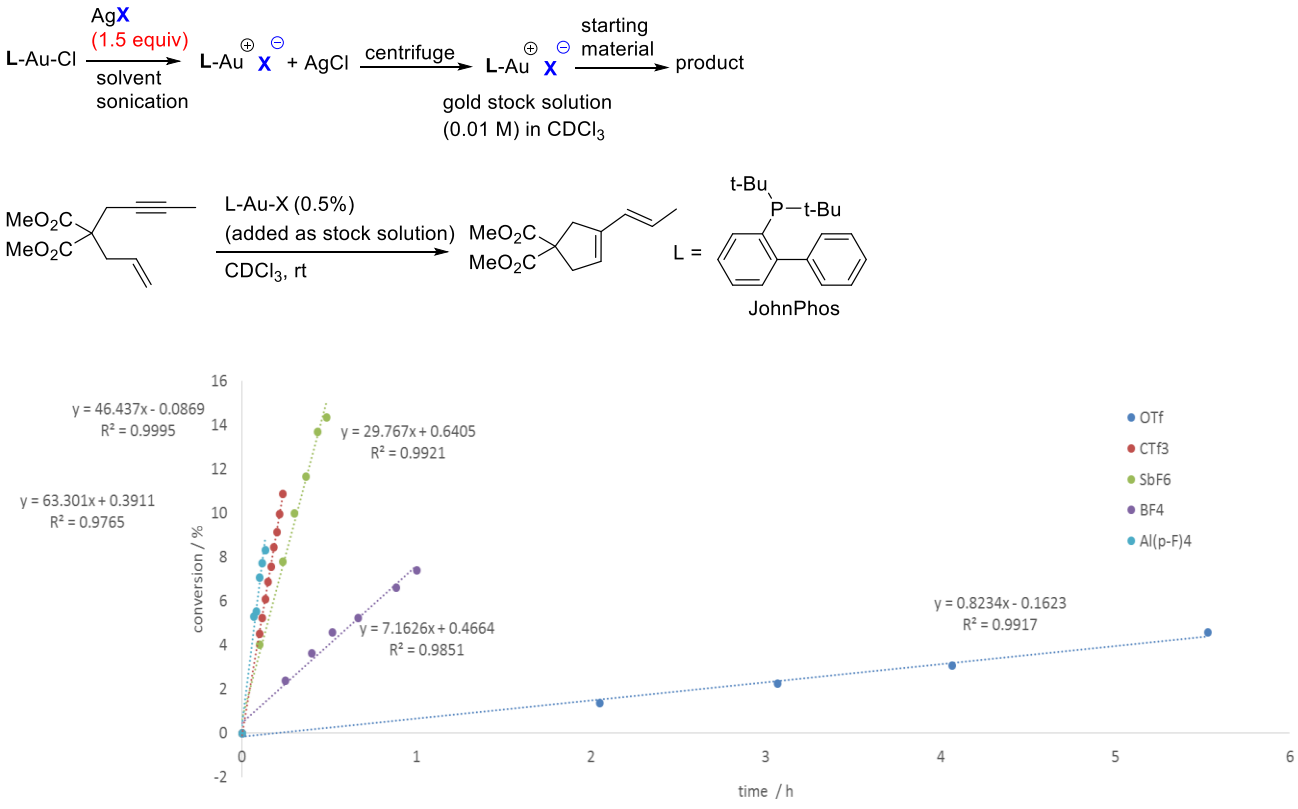

Figure S - 8. Cationic gold-catalyzed cycloisomerization of 1,6-enyne, related to Figure 6

Table S - 7. The initial reaction rate gold-catalyzed cycloisomerization of 1,6-enyne, related to Figure 6

counterion	initial rate (trial 1) ($mol{\cdot}L^{-1}h^{-1}$)	initial rate (trial 2) ($mol{\cdot}L^{-1}h^{-1}$)	initial rate (trial 3) ($mol{\cdot}L^{-1}h^{-1}$)	average relative initial reaction rate	average initial reaction rate ($mol{\cdot}L^{-1}h^{-1}$)	$\ln(k_n/k_1)$	standard deviation of $\ln(k_n/k_1)$
Triflate	0.002	0.003	0.002	0.002	0.002	-	0.00
BF_4^-	0.021	0.019	0.014	1.14	1.00	0.00	0.20
SbF_6^-	0.050	0.043	0.059	2.55	2.76	1.01	0.16
CTf_3^-	0.092	0.080	0.093	3.25	4.81	1.57	0.08
$Al[(CF_3)_3C\text{-}O)]_4^-$	0.119	0.103	0.127	7.09	6.32	1.84	0.10

Table S - 8. Cationic gold-catalyzed cycloisomerization of 1,6-enyne, related to Figure 6

counterion	Δr/ Å	$r_1^2\text{-}r_n^2$	rel. rate	$\ln(k_n/k_1)$	standard deviation
Triflate		0.00	0.14	-	0.31
BF_4^-	0.00	0.00	1.00	0.00	0.09
SbF_6^-	0.91	0.03	3.05	1.12	0.15
CTf_3^-	1.17	0.04	4.52	1.51	0.08
$Al[(CF_3)_3C\text{-}O)]_4^-$	2.13	0.05	5.97	1.79	0.10

Section 6. Supplemental References

M. J. Frisch, G.W.T., H. B. Schlegel, G. E. Scuseria, M. A. Robb, J. R. Cheeseman, G. Scalmani, V. Barone, G. A. Petersson, H. Nakatsuji, X. Li, M. Caricato, A. Marenich, J. Bloino, B. G. Janesko, R. Gomperts, B. Mennucci, H. P. Hratchian, J. V. Ortiz, A. F. Izmaylov, J. L. Sonnenberg, D. Williams-Young, F. Ding, F. Lipparini, F. Egidi, J. Goings, B. Peng, A. Petrone, T. Henderson, D. Ranasinghe, V. G. Zakrzewski, J. Gao, N. Rega, G. Zheng, W. Liang, M. Hada, M. Ehara, K. Toyota, R. Fukuda, J. Hasegawa, M. Ishida, T. Nakajima, Y. Honda, O. Kitao, H. Nakai, T. Vreven, K. Throssell, J. A. Montgomery, Jr., J. E. Peralta, F. Ogliaro, M. Bearpark, J. J. Heyd, E. Brothers, K. N. Kudin, V. N. Staroverov, T. Keith, R. Kobayashi, J. Normand, K. Raghavachari, A. Rendell, J. C. Burant, S. S. Iyengar, J. Tomasi, M. Cossi, J. M. Millam, M. Klene, C. Adamo, R. Cammi, J. W. Ochterski, R. L. Martin, K. Morokuma, O. Farkas, J. B. Foresman, and D. J. Fox (2016). Gaussian 09, Revision A.02.

Nieto-Oberhuber, C., López, S., and Echavarren, A.M. (2005). Intramolecular [4 + 2] Cycloadditions of 1,3-Enynes or Arylalkynes with Alkenes with Highly Reactive Cationic Phosphine Au(I) Complexes. J. Am. Chem. Soc. *127*, 6178-6179.

Shannon, R. (1976). Revised effective ionic radii and systematic studies of interatomic distances in halides and chalcogenides. Acta Crystallogr. A *32*, 751-767.